Collective photon emission of two correlated atoms in free space

Stefan Richter[1,2,*] Sebastian Wolf[3] Joachim von Zanthier[1,2] and Ferdinand Schmidt-Kaler[3]

[1]*AG Quantum Optics and Quantum Information, Friedrich-Alexander-Universität Erlangen-Nürnberg, Staudtstraße 1, 91058 Erlangen, Germany*

[2]*Erlangen Graduate School in Advanced Optical Technologies (SAOT), Friedrich-Alexander-Universität Erlangen-Nürnberg, Paul-Gordan-Straße 6, 91052 Erlangen, Germany*

[3]*QUANTUM, Institut für Physik, Johannes Gutenberg-Universität Mainz, Staudingerweg 7, 55128 Mainz, Germany*

(Received 9 June 2022; revised 24 October 2022; accepted 11 January 2023; published 7 March 2023)

By preparing two distant emitters in entangled Dicke states via detection of a single photon, the subsequent spatiotemporal photon emission is investigated. Depending on the parity of the established quantum state, emission patterns for the second scattered photon are observed featuring spatial superradiance as well as subradiance. We employ ultrafast single-photon resolving cameras with high spatial resolution disclosing the spatiotemporal emission characteristics. By recording the first photon in one direction and the second photon in another, revealing the spatial two-photon cross-correlation function $g^{(2)}(\mathbf{r}_1, \mathbf{r}_2)$, we characterize the collective spontaneous emission behavior of two ions in free space. We explain the observed contrast of $g^{(2)}(\mathbf{r}_1, \mathbf{r}_2)$ considering independently derived experimental parameters. Our results show how the detection of a single photon can profoundly modify the collective spontaneous emission dynamics of an atomic ensemble.

DOI: 10.1103/PhysRevResearch.5.013163

I. INTRODUCTION

Spontaneous emission of an atom can be modified by imposing boundary conditions on the vacuum field as in cavity quantum electrodynamics (QED) [1]. Another option to change the spatiotemporal characteristics of spontaneous decay exploits particle-particle correlations of ensembles of atoms in free space leading to collective light emission known as superradiance and subradiance [2,3]. The correlations among the emitters may be induced by interactions, e.g., using the Coulomb or Rydberg interaction [4–6], or via exchange of virtual photons in the case of small separations [7–13]. An alternative route proposed for generating correlations among emitters relies on the measurement of photons excluding which-path information [14–17]. Erasing which-path information has been realized by mixing the photons in a beam splitter [18–22] or detecting them in the far field [23,24]. So far, producing entangled states via projective measurements of photons has been realized with ions [18,23,24], neutral atoms [19,25], NV centers [20], and quantum dots [21,22].

Based on the direction of detection of a first scattered photon, the generation of Dicke states has been suggested for two atoms initially in the excited state [15,16]. Depending on the parity of the Dicke state, either superradiant or subradiant spatial emission patterns are predicted for the subsequently radiated photon [26]. However, in all experiments so far, single spatial light modes have been picked out for the measurement of the scattered photons, inhibiting the observation of genuine spatial emission patterns of the emitted radiation. Here, we report on experimentally projecting two distant ions, i.e., with no direct optical interaction or electronic state coupling, onto entangled Dicke states via photon detection followed by the observation of the collective spatial emission patterns of the subsequently emitted photon.

II. THEORY

Recording two photons scattered from an atomic ensemble amounts to measuring the second-order photon correlation function. For a pair of laser-driven two-level atoms, the normalized second-order photon correlation function can be derived from a master equation approach [15]. In the case of coincident photon detection, the second-order photon cross-correlation function reads

$$g^{(2)}(\mathbf{r}_1, \mathbf{r}_2, \tau = 0) = \frac{(1+s)^2 \cos^2\left[\frac{\delta(\mathbf{r}_1)-\delta(\mathbf{r}_2)}{2}\right]}{[1+s+\cos\delta(\mathbf{r}_1)][1+s+\cos\delta(\mathbf{r}_2)]}. \quad (1)$$

Here, s denotes the saturation parameter of the atomic transition $|g\rangle \leftrightarrow |e\rangle$ and $\delta(\mathbf{r}) = k_L \hat{\mathbf{r}} \cdot \mathbf{d}$ the optical phase accumulated by a photon recorded at position $\mathbf{r}$ if scattered by atom 1 with respect to a photon scattered by atom 2, with $\mathbf{d}$ the distance vector of the two atoms and k_L the laser wave number. Note that $g^{(2)}(\mathbf{r}_1, \mathbf{r}_2, \tau = 0)$ depends on both the phase accumulated by the first photon detected at $\mathbf{r}_1$ and the phase of the second photon recorded at $\mathbf{r}_2$. Here, $g^{(2)}(\mathbf{r}_1, \mathbf{r}_2, \tau = 0)$ varies with $\delta(\mathbf{r}_2)$ if the second detector at position $\mathbf{r}_2$ is moved along an axis parallel to the interion distance vector $\mathbf{d}$, with an initial phase depending on $\delta(\mathbf{r}_1)$. In addition, $g^{(2)}(\mathbf{r}_1, \mathbf{r}_2, \tau =$

*stefan.michael.richter@fau.de

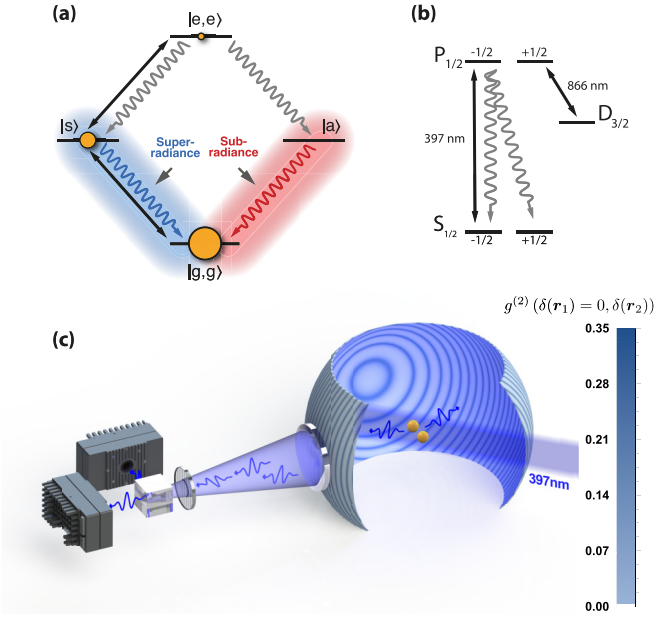

FIG. 1. (a) Level scheme of the two-ion system in the Dicke basis. Starting from $|e,e\rangle$ and measuring a spontaneously emitted photon (gray) in the far field at $\mathbf{r}_1$ such that $\delta(\mathbf{r}_1) = n2\pi$, $n \in N$, the two-ion system is projected into the symmetric Dicke state $|s\rangle = [\exp(-i\phi)\,|e,g\rangle + \exp(i\phi)\,|g,e\rangle]/\sqrt{2}$, with $\phi = (\mathbf{k}_L \cdot \mathbf{d})/2$. From there, it emits a second photon with a spatial pattern corresponding to spatial superradiance (blue). Contrary, measuring a photon at $\mathbf{r}_1$ with $\delta(\mathbf{r}_1) = (2n+1)\pi$, $n \in N$, the system is projected into the antisymmetric Dicke state $|a\rangle = [\exp(-i\phi)\,|e,g\rangle - \exp(i\phi)\,|g,e\rangle]/\sqrt{2}$, and the second photon is emitted with a spatial distribution corresponding to spatial subradiance (red). Laser light (black) couples to symmetric Dicke states $|g,g\rangle$, $|s\rangle$, and $|e,e\rangle$ only; hence, for low laser saturation, essentially $|g,g\rangle$ and $|s\rangle$ are populated, whereas $|e,e\rangle$ is hardly occupied (yellow circles). (b) Relevant levels and transitions of $^{40}Ca^+$, driven by a red-detuned laser ~397 nm and a resonant laser ~866 nm to obtain continuous fluorescence and laser cooling. (c) Two $^{40}Ca^+$ ions are trapped and continuously excited on the $S_{1/2}$-$P_{1/2}$ transition while the scattered light is collected by a lens and, after passing a polarization filter, fed into a Hanbury-Brown and Twiss setup using two microchannel plate (MCP) cameras to measure $g^{(2)}(\mathbf{r}_1, \mathbf{r}_2, \tau)$. The sphere around the two ions sketches the spatial pattern of $g^{(2)}(\mathbf{r}_1, \mathbf{r}_2, \tau = 0)$ as a function of $\mathbf{r}_2$ for $\delta(\mathbf{r}_1) = 0.1\pi$.

0) predicts a maximum detection probability for the second photon at $\delta(\mathbf{r}_2) = 0$ if the first photon has also been recorded at $\delta(\mathbf{r}_1) = 0$, corresponding to spatial superradiance [17,26]. Oppositely, $g^{(2)}(\mathbf{r}_1, \mathbf{r}_2, \tau = 0)$ features at $\delta(\mathbf{r}_2) = 0$ a minimum detection probability for the second photon if the first photon has been recorded at $\delta(\mathbf{r}_1) = \pi$, corresponding to spatial subradiance [see Fig. 1(a)].

III. EXPERIMENT

We employ a pair of $^{40}Ca^+$ ions to investigate such collective emission behavior in free space, held in a segmented linear Paul trap with trap frequencies $\omega_{(\mathrm{ax,\,rad1,\,rad2})}/2\pi = (0.76, 1.275, 1.568)$ MHz for the axial and the two radial modes, respectively. The trapped ions are continuously excited and laser-cooled by laser light near the $S_{1/2}$-$P_{1/2}$ transition at 397 nm, whereas a laser ~866 nm is pumping out of the long-lived $D_{3/2}$ state, see Fig. 1(b). A quantization axis is defined by a magnetic field $B = 0.62$ mT oriented vertical to the detection plane and coinciding with the polarization direction of the exciting laser. A $f/1.6$ lens system collects 2.5% of the photons scattered by the ions on the $S_{1/2}$-$P_{1/2}$ transition. After passing a polarization filter, vertical to the detection plane to ensure indistinguishably of the scattered photons, they are fed into a Hanbury-Brown and Twiss setup consisting of a nonpolarizing 50/50 beam splitter and two synchronized microchannel plate (MCP) camera detectors with 1000×1000 virtual spatial bins and a timing resolution of 50 ps, thus combining both high spatial and high temporal resolution, see Fig. 1(c). As each of the MCPs has a dead time of 600 ns, we use two of these detectors to resolve $g^{(2)}(\mathbf{r}_1, \mathbf{r}_2, \tau)$ to better than the coherence time of the ion given by $\tau_{P_{1/2}} = 6.9$ ns [27].

We record the photon stream from the ion pair in the far field on the MCP cameras. At a single photon count rate of ~7 kHz for the first detector and ~8.5 kHz for the second one, leading to a coincidence rate of ~68 mHz per bin, we record data for ~205 h net. The total count rate of ~15.5 kHz is ~30% lower than theoretically predicted, where the discrepancy results from experimental artifacts like surface reflections, abberations, misalignments, and overfilling of the detector area. To increase the statistics per bin, the two-dimensional 1000×1000 spatial dataset of each frame of each MCP camera is reduced to 1×96 bins, taking advantage of the fact that the relevant spatial modulation of $g^{(2)}(\mathbf{r}_1, \mathbf{r}_2, \tau)$ occurs in one dimension only, i.e., parallel to the ion distance vector $\mathbf{d}$. We choose time bins of 2.5 ns, shorter than $\tau_{P_{1/2}}$ but significantly longer than the time resolution of the MCP cameras, for again increasing the statistics per bin. Finally, the two-photon correlation is stored in a data structure with $96 \times 96 \times 38$ bins, encoding the position of the first (the second) photon detection event at $\mathbf{r}_1$ (at $\mathbf{r}_2$) and the photon arrival time difference τ, with each entry of the data structure filled on average by ~20 photon correlation events. From these data (available online [28]), we compute the spatiotemporal correlation $g^{(2)}(\mathbf{r}_1, \mathbf{r}_2, \tau)$

IV. RESULTS

Let us now discuss the rich spatial and temporal phenomena in the collective light emission of the two correlated ions as measured by the two-photon correlation function $g^{(2)}(\mathbf{r}_1, \mathbf{r}_2, \tau)$: Selecting from the total dataset four different values for the first photon emission direction, i.e., $\delta(\mathbf{r}_1) = 0.1\pi, 0.7\pi, 1.0\pi, 1.4\pi$, the correlation function is measured as a function of the direction of emission of the second photon $\delta(\mathbf{r}_2)$, see Figs. 2(a)(i)–2(a)(iv). The plots demonstrate that, depending on the direction of emission of the first photon, different phases of Dicke states are projectively prepared, which is proven by the altered emission for the second photon. The field of observation for the second photon, given by the size of our Hanbury-Brown and Twiss camera active area, captures ~10 periods of $\delta(\mathbf{r}_2)$, i.e., 10 modulations of $g^{(2)}(\mathbf{r}_1, \mathbf{r}_2, \tau)$. Note that the contrast of the modulations is most pronounced for photon emission events with small photon arrival time differences $\tau \simeq 0$, due to the short

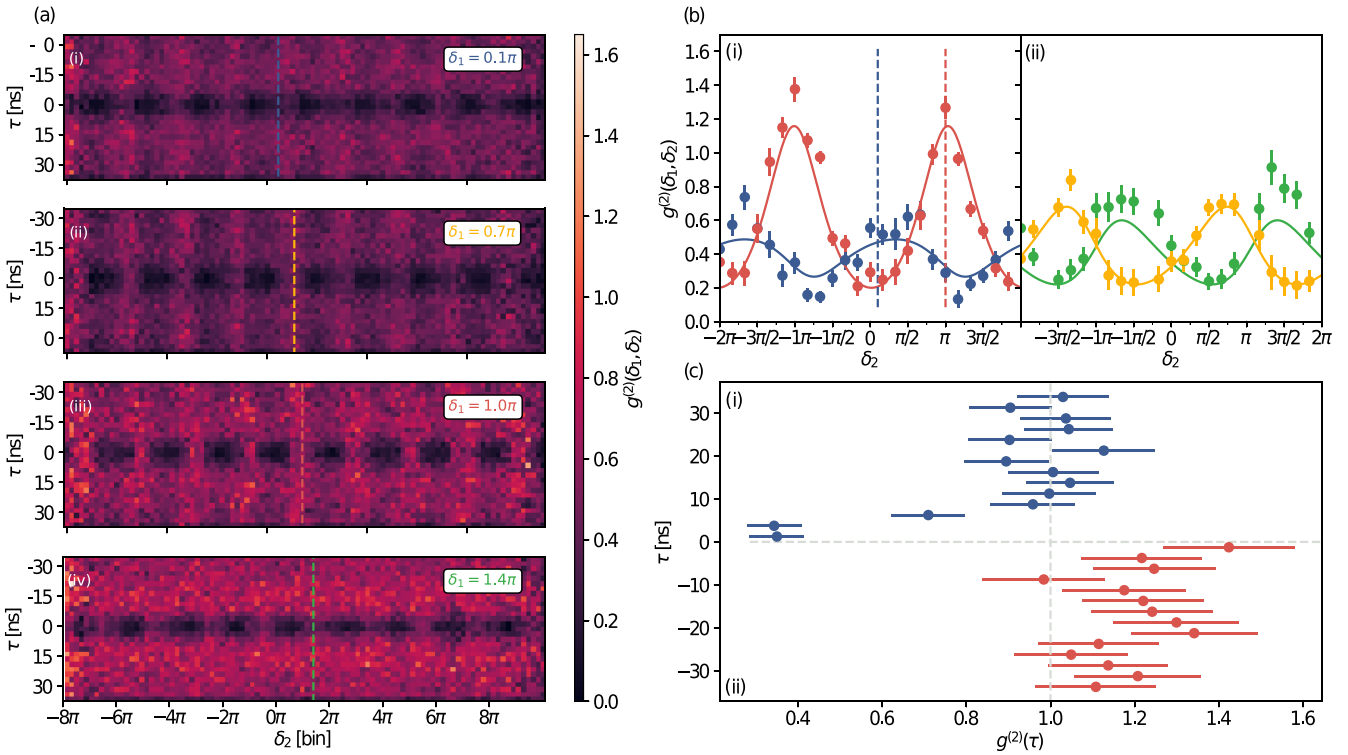

FIG. 2. (a) Histograms of the spatiotemporal photon (cross-)correlation function $g^{(2)}(\mathbf{r}_1, \mathbf{r}_2, \tau)$ as a function of $\delta(\mathbf{r}_2)$ (horizontal axis) and photon arrival time difference τ (vertical axis) for different directions of the first photon detection event (indicated as doted lines): (i) $\delta(\mathbf{r}_1) = 0.1\pi$, (ii) $\delta(\mathbf{r}_1) = 0.7\pi$, (iii) $\delta(\mathbf{r}_1) = 1.0\pi$, and (iv) $\delta(\mathbf{r}_1) = 1.4\pi$. (b) Cuts of the histograms at $\tau = 0$, binned to $\delta(\mathbf{r}_2) \in [-2\pi, +2\pi]$: (i) spatial superradiance (blue dots) and subradiance (red dots) observed in the direction $\delta(\mathbf{r}_2) \approx 0$ in the case that $\delta(\mathbf{r}_1) = 0.1\pi$ and $\delta(\mathbf{r}_1) = 1.05\,\pi$, respectively. The asymmetry of the curve with $\delta(\mathbf{r}_1) = 0.1\pi$ results from the finite spatial binning, not allowing to select from the data a bin with precisely $\delta(\mathbf{r}_1) = 0\pi$; and (ii) intermediate regimes between spatial superradiance and subradiance for the second spontaneously scattered photon in the case that $\delta(\mathbf{r}_1) = 0.7\pi$ (yellow dots) and $\delta(\mathbf{r}_1) = 1.4\pi$ (green dots). Fitting the histograms by use of Eq. (2) leads to the four correlation functions displayed as solid lines (in blue, red, yellow, and green, respectively); the position of the corresponding first photon detection is indicated in (i) by dashed vertical lines. (c) Temporal autocorrelation function $g^{(2)}(\tau)$: (i) Photon antibunching with $g^{(2)}(\tau) = 0.29(6)$ is observed for $\delta(\mathbf{r}_1) = \delta(\mathbf{r}_2) = 0.1\pi$ [at blue vertical dotted line in (b)(i)]; and (ii) photon bunching with $g^{(2)}(\tau) = 1.42(16)$ is measured for $\delta(\mathbf{r}_1) = \delta(\mathbf{r}_2) = 1.0\pi$ [red vertical dotted line in (b)(i)]. Error bars correspond to one statistical standard deviation for all subplots.

natural lifetime of the $P_{1/2}$ exited state. Moreover, the phase of the modulations changes with $\delta(\mathbf{r}_1)$, i.e., depending on the emission direction of the first photon, compare Figs. 2(a)(i)–2(a)(iv). We further dwell into the spatial characteristics of the collective emission by plotting cuts of the histograms at the value of $\tau = 0$, binned to only two periods $\delta(\mathbf{r}_2) \in [-2\pi, +2\pi]$, see Fig. 2(b). The photon correlations show distinct spatial emission patterns for the second spontaneously emitted photon depending on $\delta(\mathbf{r}_1)$, i.e., the position of the first photon detection event and thus the corresponding Dicke state parity. We recognize a pattern with maximum emission probability for the second photon in the direction $\delta(\mathbf{r}_2) \approx 0$ in the case that the first photon has been recorded at $\delta(\mathbf{r}_1) = 0.1\,\pi$ [blue dots in Fig. 2(b)(i)]. For this setting, the two-ion system has been projected approximately into the symmetric Dicke state $|s\rangle = [\exp(-i\phi)\,|e, g\rangle + \exp(i\phi)\,|g, e\rangle]/\sqrt{2}$, with $\phi = (\mathbf{k}_L \cdot \mathbf{d})/2$, i.e., we observe the regime of spatial superradiance [15,17,26]. By contrast, a pattern with minimum emission probability in the direction $\delta(\mathbf{r}_2) \approx 0$ is obtained if the first photon has been recorded at $\delta(\mathbf{r}_1) = 1.0\,\pi$ [red dots in Fig. 2(b)(i)]. In this case, the two-ion system has been projected approximately into the antisymmetric Dicke state $|a\rangle = [\exp(-i\phi)\,|e, g\rangle - \exp(i\phi)\,|g, e\rangle]/\sqrt{2}$, corresponding to the regime of spatial subradiance (see also Fig. 1). Note that the slight deviation of $\delta(\mathbf{r}_1)$ from the more transparent value $\delta(\mathbf{r}_1) = 0$ results from the spatial binning process outlined above, see blue dots in Fig. 2(b)(i). However, this does not impair the clear experimental observation of largely different emission patterns for the second photon, depending on the detection position of the first photon $\delta(\mathbf{r}_1)$.

To model the experimentally measured data, we extend Eq. (1) by including the Debye-Waller factor $f^{\mathbf{r}}_{\mathrm{DWF}}$, which describes the residual motion of the trapped ions as well as the momentum transfer induced onto the two-ion system by the absorbed and emitted photons. Additionally, we consider an offset of $\Delta \approx 0.2$, resulting from dark counts and events when the ions decay into the metastable $D_{3/2}$ state and are pumped back into the fluorescence cycle by the laser ∼866 nm [29] (∼6.5 % of the deexcitations). The offset also includes a loss of contrast due to the convolutions in the temporal and spatial binning process outlined above. Thus, from Eq. (1), we find the theoretical model

function:

$$g^{(2)}(\mathbf{r}_1, \mathbf{r}_2, \tau = 0) = \frac{(1+s)^2 \cos^2\left[\frac{\delta(\mathbf{r}_1)-\delta(\mathbf{r}_2)}{2}\right] f_{\mathrm{DWF}}^{\mathbf{r}_1} f_{\mathrm{DWF}}^{\mathbf{r}_2}}{\left[1+s+\cos\delta(\mathbf{r}_1) f_{\mathrm{DWF}}^{\mathbf{r}_1}\right]\left[1+s+\cos\delta(\mathbf{r}_2) f_{\mathrm{DWF}}^{\mathbf{r}_2}\right]} + \Delta, \tag{2}$$

where $f_{\mathrm{DWF}}^{\mathbf{r}_i}$ is given by [30]

$$f_{\mathrm{DWF}}^{\mathbf{r}_i} = \exp\left[-\frac{\hbar q_x^2(\mathbf{r}_i)}{m\omega_{\mathrm{roc}_x}}\left(\langle N_{\mathrm{roc}_x}\rangle + \frac{1}{2}\right) - \frac{\hbar q_y^2(\mathbf{r}_i)}{m\omega_{\mathrm{roc}_y}}\left(\langle N_{\mathrm{roc}_y}\rangle + \frac{1}{2}\right) - \frac{\hbar q_z^2(\mathbf{r}_i)}{m\omega_b}\left(\langle N_b\rangle + \frac{1}{2}\right)\right]. \tag{3}$$

Here, $q_\alpha(\mathbf{r}_i)$, $i = 1, 2$, describes the projection of the momentum transfer vector $\mathbf{q}(\mathbf{r}_i) = \mathbf{k}_L - k_L\hat{\mathbf{r}}_i$ onto the basis axis $\alpha = x, y, z$ of the underlying vibrational modes ω_κ occupied by $\langle N_\kappa\rangle$ phonons, where ω_κ are the frequencies of the relevant vibrational modes $\kappa = \mathrm{roc}_x, \mathrm{roc}_y, b$. Note that, for the investigated two-ion system, out of the six possible modes, only the contrast-reducing modes have to be considered, namely, the breathing mode ω_b, affecting the interion distance, and the two rocking modes ω_{roc_x} and ω_{roc_y}, acting perpendicular to the ion distance vector $\mathbf{d}$ and describing the shear movement of the ions along two orthogonal axes. For the investigated two-ion system, the Debye-Waller factors calculate to $f_{\mathrm{DWF}}^{\mathbf{r}_1} \approx f_{\mathrm{DWF}}^{\mathbf{r}_2} = 0.51$, considering the chosen angle of $\alpha \approx 135^\circ$ between the laser wave vector $\mathbf{k}_L$ and the detector positions $\mathbf{r}_i$, $i = 1, 2$, as well as the residual phonon numbers $\langle N_b\rangle \approx 15$, $\langle N_{\mathrm{roc}_x}\rangle \approx 9$, and $\langle N_{\mathrm{roc}_y}\rangle \approx 7$ after cooling the two-ion system to the Doppler limit. The saturation parameter of the cooling laser is determined to $s = 0.65$, derived experimentally independently from the Rabi oscillations of the autocorrelation function $g^{(2)}(\tau)$ using a single trapped ion for different laser powers [31]. With those values fixed, the only adjustable parameter of the model function remains the phase $\delta(\mathbf{r}_1)$ of the first recorded photon which is determined by a least square fit. The corresponding results for $g^{(2)}(\mathbf{r}_1, \mathbf{r}_2, \tau = 0)$ for each of the four phases $\delta(\mathbf{r}_1)$ with $\Delta = 0.2$ display remarkably good agreement to the data, see Fig. 2(b).

Turning now to the discussion of the temporal features in the measured photon correlation function $g^{(2)}$, we observe that the photon autocorrelation function $g^{(2)}(\mathbf{r}_1, \mathbf{r}_1, \tau = 0)$ displays antibunching for $\delta(\mathbf{r}_1) = \delta(\mathbf{r}_2) = 0.1\,\pi$ and bunching for $\delta(\mathbf{r}_1) = \delta(\mathbf{r}_2) = 1.0\,\pi$, see Fig. 2(c). Such spatial variation of the photon statistics stems from the fact that laser light couples only the symmetric states $|g, g\rangle$, $|s\rangle$, and $|e, e\rangle$ of the two-ion system, not the antisymmetric state $|a\rangle$ [15]. Thus, for low saturation of the two-ion system, essentially only the two-ion ground state $|g, g\rangle$ is occupied, whereas the state $|s\rangle$ is much less populated and the state $|e, e\rangle$ hardly at all. For the spatial direction $\delta(\mathbf{r}_1) = \delta(\mathbf{r}_2) \approx 0$, i.e., when the photons decay along the symmetric decay channels $|e, e\rangle \rightarrow |s\rangle$ or $|s\rangle \rightarrow |g, g\rangle$, a recorded photon will thus in most cases originate from the transition $|s\rangle \rightarrow |g, g\rangle$, see Fig. 1. Hence, after detection of a photon, the system must first be reexcited to the state $|s\rangle$ before the next photon can be recorded. The resulting time lag leads to antibunching of the photon stream [32]. By contrast, for the two detectors located at $\delta(\mathbf{r}_1) = \delta(\mathbf{r}_2) \approx \pi$, the autocorrelation $g^{(2)}(\mathbf{r}_1, \mathbf{r}_1, \tau)$ measures only photons decaying along the antisymmetric decay channel $|e, e\rangle \rightarrow |a\rangle \rightarrow |g, g\rangle$ (see Fig. 1), giving rise to two consecutive photon emissions and therefore to bunching of the scattered photons [32]. Combining both the spatial and the temporal aspects of the collective light emission of the two-ion system, we recognize that the maximum of superradiance observed at a position $\delta(\mathbf{r}_2) = \delta(\mathbf{r}_1) \approx 0$ is accompanied by photon antibunching, whereas the maximum of spatial subradiance appearing at $\delta(\mathbf{r}_2) = \delta(\mathbf{r}_1) \approx \pi$ goes together with bunching of the photon stream.

V. CONCLUSION

We conclude that the collective spontaneous emission behavior of a correlated atomic array in free space features a variety of astonishing properties, i.e., spatial superradiance and subradiance accompanied by photon antibunching and bunching, respectively. We observe these genuine features of collective spontaneous emission with the most elementary building block of photon emitters, a pair of noninteracting trapped ions. Already, this conceptually simple setup leads to a great wealth of spatiotemporal emission phenomena which we experimentally characterized by measuring the second-order photon correlation function $g^{(2)}(\mathbf{r}_1, \mathbf{r}_2, \tau)$. Neglecting the phase dependency and focusing only on the spatial frequency of $g^{(2)}(\mathbf{r}_1, \mathbf{r}_2, \tau = 0)$ in the case of coincident photon detection allows moreover the determination of the orientation and separation of the two ions, i.e., imaging of the sample [33]. By use of our simple and versatile model system of two ions, we can trace back how quantum cooperativity is established via projective measurements. We model the observed behavior via a master equation approach, considering independently derived experimental parameters. In the future, we will explore collective spontaneous emission for crystals with a larger number of ions, eventually extending to two-dimensional arrays, aiming for projective preparation and imaging of long-lived entangled states.

Source data for the plots shown are provided online [28]. The experimental data that support the findings of this study are available from the corresponding author upon reasonable request.

ACKNOWLEDGMENTS

We thank Photonscore GmbH, Brenneckestraße 20, 39118 Magdeburg, Germany, for providing the synchronized MCP camera system [34] and André Weber for the initial calibration and characterization of the MPC systems. J.v.Z. thanks Ralf Palmisano for making contact to Photonscore GmbH. We acknowledge funding by the Deutsche Forschungsgemeinschaft within the TRR 306 QuCoLiMa ("Quantum Cooperativity of Light and Matter")—Project-ID 429529648. S.R. and J.v.Z. acknowledge support from the Erlangen Graduate School in Advanced Optical Technologies (SAOT).

[1] S. Haroche and J.-M. Raimond, *Exploring the Quantum: Atoms, Cavities, and Photons* (Oxford University Press, Oxford, 2006).

[2] R. H. Dicke, Coherence in spontaneous radiation processes, Phys. Rev. **93**, 99 (1954).

[3] M. Gross and S. Haroche, Superradiance: An essay on the theory of collective spontaneous emission, Phys. Rep. **93**, 301 (1982).

[4] C. Monroe, D. M. Meekhof, B. E. King, W. M. Itano, and D. J. Wineland, Demonstration of a Fundamental Quantum Logic Gate, Phys. Rev. Lett. **75**, 4714 (1995).

[5] T. Monz, P. Schindler, J. T. Barreiro, M. Chwalla, D. Nigg, W. A. Coish, M. Harlander, W. Hänsel, M. Hennrich, and R. Blatt, 14-Qubit Entanglement: Creation and Coherence, Phys. Rev. Lett. **106**, 130506 (2011).

[6] S. Ebadi, T. T. Wang, H. Levine, A. Keesling, G. Semeghini, A. Omran, D. Bluvstein, R. Samajdar, H. Pichler, W. Wei Ho *et al.*, Quantum phases of matter on a 256-atom programmable quantum simulator, Nature (London) **595**, 227 (2021).

[7] R. G. DeVoe and R. G. Brewer, Observation of Superradiant and Subradiant Spontaneous Emission of Two Trapped Ions, Phys. Rev. Lett. **76**, 2049 (1996).

[8] A. González-Tudela, C.-L. Hung, D. E. Chang, J. I. Cirac, and H. J. Kimble, Subwavelength vacuum lattices and atom–atom interactions in two-dimensional photonic crystals, Nat. Photonics **9**, 320 (2015).

[9] G. Facchinetti, S. D. Jenkins, and J. Ruostekoski, Storing Light with Subradiant Correlations in Arrays of Atoms, Phys. Rev. Lett. **117**, 243601 (2016).

[10] E. Shahmoon, D. S. Wild, M. D. Lukin, and S. F. Yelin, Cooperative Resonances in Light Scattering from Two-Dimensional Atomic Arrays, Phys. Rev. Lett. **118**, 113601 (2017).

[11] A. Asenjo-Garcia, M. Moreno-Cardoner, A. Albrecht, H. J. Kimble, and D. E. Chang, Exponential Improvement in Photon Storage Fidelities using Subradiance and "Selective Radiance" in Atomic Arrays, Phys. Rev. X **7**, 031024 (2017).

[12] J. Rui, D. Wei, A. Rubio-Abadal, S. Hollerith, J. Zeiher, D. M. Stamper-Kurn, C. Gross, and I. Bloch, A subradiant optical mirror formed by a single structured atomic layer, Nature (London) **583**, 369 (2020).

[13] G. Ferioli, A. Glicenstein, F. Robicheaux, R. T. Sutherland, A. Browaeys, and I. Ferrier-Barbut, Laser-Driven Superradiant Ensembles of Two-Level Atoms near Dicke Regime, Phys. Rev. Lett. **127**, 243602 (2021).

[14] C. Cabrillo, J. I. Cirac, P. Garcia-Fernandez, and P. Zoller, Creation of entangled states of distant atoms by interference, Phys. Rev. A **59**, 1025 (1999).

[15] C. Skornia, J. von Zanthier, G. S. Agarwal, E. Werner, and H. Walther, Nonclassical interference effects in the radiation from coherently driven uncorrelated atoms, Phys. Rev. A **64**, 063801 (2001).

[16] C. Thiel, J. von Zanthier, T. Bastin, E. Solano, and G. S. Agarwal, Generation of Symmetric Dicke States of Remote Qubits with Linear Optics, Phys. Rev. Lett. **99**, 193602 (2007).

[17] S. Oppel, R. Wiegner, G. S. Agarwal, and J. von Zanthier, Directional Superradiant Emission from Statistically Independent Incoherent Nonclassical and Classical Sources, Phys. Rev. Lett. **113**, 263606 (2014).

[18] D. L. Moehring, P. Maunz, S. Olmschenk, K. C. Younge, D. N. Matsukevich, L.-M. Duan, and C. Monroe, Entanglement of single-atom quantum bits at a distance, Nature (London) **449**, 68 (2007).

[19] J. Hofmann, M. Krug, N. Ortegel, L. Gérard, M. Weber, W. Rosenfeld, and H. Weinfurter, Heralded entanglement between widely separated atoms, Science **337**, 72 (2012).

[20] H. Bernien, B. Hensen, W. Pfaff, G. Koolstra, M. S. Blok, L. Robledo, T. H. Taminiau, M. Markham, D. J. Twitchen, L. Childress, and R. Hanson, Heralded entanglement between solid-state qubits separated by three metres, Nature (London) **497**, 86 (2013).

[21] A. Delteil, Z. Sun, W.-b. Gao, E. Togan, S. Faelt, and A. Imamoğlu, Generation of heralded entanglement between distant hole spins, Nat. Phys. **12**, 218 (2016).

[22] R. Stockill, M. J. Stanley, L. Huthmacher, E. Clarke, M. Hugues, A. J. Miller, C. Matthiesen, C. Le Gall, and M. Atatüre, Phase-Tuned Entangled State Generation between Distant Spin Qubits, Phys. Rev. Lett. **119**, 010503 (2017).

[23] L. Slodička, G. Hétet, N. Röck, P. Schindler, M. Hennrich, and R. Blatt, Atom-Atom Entanglement by Single-Photon Detection, Phys. Rev. Lett. **110**, 083603 (2013).

[24] G. Araneda, D. B. Higginbottom, L. Slodička, Y. Colombe, and R. Blatt, Interference of Single Photons Emitted by Entangled Atoms in Free Space, Phys. Rev. Lett. **120**, 193603 (2018).

[25] R. McConnell, H. Zhang, J. Hu, S. Ćuk, and V. Vuletić, Entanglement with negative Wigner function of almost 3,000 atoms heralded by one photon, Nature (London) **519**, 439 (2015).

[26] R. Wiegner, J. von Zanthier, and G. S. Agarwal, Quantum-interference-initiated superradiant and subradiant emission from entangled atoms, Phys. Rev. A **84**, 023805 (2011).

[27] M. Hettrich, T. Ruster, H. Kaufmann, C. F. Roos, C. T. Schmiegelow, F. Schmidt-Kaler, and U. G. Poschinger, Measurement of Dipole Matrix Elements with a Single Trapped Ion, Phys. Rev. Lett. **115**, 143003 (2015).

[28] S. Richter, S. Wolf, J. von Zanthier, and F. Schmidt-Kaler, Dataset for the plots of "Collective photon emission patterns from two atoms in free space," Friedrich-Alexander-Universität Erlangen-Nürnberg (2022), doi: 10.22000/560.

[29] M. Ramm, T. Pruttivarasin, M. Kokish, I. Talukdar, and H. Häffner, Precision Measurement Method for Branching Fractions of Excited $P_{1/2}$ States Applied to $^{40}Ca^{+}$, Phys. Rev. Lett. **111**, 023004 (2013).

[30] W. M. Itano, J. C. Bergquist, J. J. Bollinger, D. J. Wineland, U. Eichmann, and M. G. Raizen, Complementarity and Young's interference fringes from two atoms, Phys. Rev. A **57**, 4176 (1998).

[31] F. Diedrich and H. Walther, Nonclassical Radiation of a Single Stored Ion, Phys. Rev. Lett. **58**, 203 (1987).

[32] S. Wolf, S. Richter, J. von Zanthier, and F. Schmidt-Kaler, Light of Two Atoms in Free Space: Bunching or Antibunching? Phys. Rev. Lett. **124**, 063603 (2020).

[33] S. Richter, S. Wolf, J. von Zanthier, and F. Schmidt-Kaler, Imaging Trapped Ion Structures via Fluorescence Cross-Correlation Detection, Phys. Rev. Lett. **126**, 173602 (2021).

[34] https://photonscore.de.